PHYSICAL REVIEW B **72**, 224102 (2005)

Effect of pressure on the structural properties and Raman modes of $LiCoO_2$

X. Wang,[1] I. Loa,[1] K. Kunc,[1,2] K. Syassen,[1,*] and M. Amboage[3]
[1]*Max-Planck-Institut für Festkörperforschung, Heisenbergstraße 1, D-70569 Stuttgart, Germany*
[2]*Institut des Nanosciences de Paris, CNRS and Université Pierre et Marie Curie, 140 rue de Lourmel, F-75015 Paris, France*
[3]*European Synchrotron Radiation Facility, Boîte Postale 220, F-38043 Grenoble, France*

(Received 14 September 2005; published 5 December 2005)

The high-pressure behavior of fully intercalated lithium cobaltite, $LiCoO_2$, has been investigated by angle-dispersive synchrotron x-ray powder diffraction and Raman spectroscopy. The layered structure ($R\bar{3}m$) is found to exist up to at least 26 GPa. From refinements of x-ray diffraction patterns information is derived on changes of Co-O and Li-O bond lengths under pressure. The stability of the ambient-pressure phase is confirmed by Raman spectroscopy. The pressure coefficients for the A_{1g} and E_g Raman modes and their mode-Grüneisen parameters are reported as well as qualitative observations concerning unusual changes in width and intensity of the Raman lines under pressure. The obtained high-pressure structural and vibrational properties are compared to results of *ab initio* calculations.

DOI: 10.1103/PhysRevB.72.224102 PACS number(s): 61.50.Ks, 61.50.Ah, 78.30.Hv, 82.47.Aa

I. INTRODUCTION

Lithium cobaltite has the most remarkable property of allowing a reversible removal and reinsertion of lithium.[1,2] Rechargeable batteries using Li_xCoO_2 cathodes exhibit the highest energy density among batteries using similar transition metal oxides (e.g., $LiNiO_2$ or $LiVO_2$).[1,3–5] Consequently, a large amount of work has been devoted to studying the Li intercalation process which includes extensive modeling of the structural properties, the insulator to metal transition, and the electrochemical parameters of the Li-deficient cobaltite.

The fully "lithiated" compound with stoichiometry $LiCoO_2$ crystallizes in two modifications.[6–14] The common form (Fig. 1), synthesized at 850 °C, adopts a layered α-$NaFeO_2$-type structure, which has space group $R\bar{3}m$ and $Z=1$ formula units in the rhombohedral cell.[8–13] The second form (synthesized at 400 °C) is cubic (space group $Fd\bar{3}m$), and it is related to the spinel-type structure.[6,7,15] The main structural difference between the layered and cubic forms of $LiCoO_2$ is how cations are distributed over octahedral interstitial sites of a distorted cubic-close-packed oxygen lattice (for a detailed discussion see, e.g., Ref. 16). The layered modification is known to be the more stable of the two,[17] although their energies are very close.[16]

The layered $LiCoO_2$ is an insulator with an optical gap of about 2 eV. Spectroscopic studies along with theory-supported interpretations have provided us with a basic picture of the electronic structure.[16,18–20] Briefly, the formal oxidation state of cobalt is 3+, corresponding to a d^6 configuration. The Co ions adopt a low-spin state. Within a molecular-orbital picture of the CoO_6 octahedral unit, three t_{2g} orbitals are fully occupied; they form the top of the valence band. The optical gap results from the splitting between weakly bonding t_{2g} and antibonding e_g^* states.[18,19] The conventional one-electron band structure approach is considered to be basically adequate for the description of $LiCoO_2$.[19]

In this paper we report the effects of pressure on structural and vibrational properties of layered $LiCoO_2$ as investigated by synchrotron x-ray diffraction and Raman spectroscopy, respectively. Little experimental and theoretical work has dealt with the behavior of $LiCoO_2$ or related compounds at high pressure. Based on *ab initio* calculations for $LiCoO_2$, a phase transition from the layered to a cubic phase was predicted to occur at around 3 GPa.[16] This kind of transition was not observed in our experiments. Instead, at room temperature the layered structure was found to exist up to at least 26 GPa. Our structural studies provide information on the compressibilities and distortions of the LiO_6 and CoO_6 octahedra (cf. Fig. 1). From high-pressure Raman spectra we have determined the mode-Grüneisen parameters of the two Raman-allowed zone-center optical modes. With increasing pressure we observed pronounced intensity changes of the two Raman modes; such an effect may be related to a pressure-induced change in the electronic excitation spectrum. We compare the experimental high-pressure structural and vibrational properties to results of *ab initio* calculations performed within the density functional theory.

II. EXPERIMENTAL METHODS

The sample of $LiCoO_2$ used for the present study was a commercial product (Merck) with stated metal purity of >99.6%. For high-pressure x-ray diffraction experiments, the sample was ground to a fine powder and then loaded into a diamond anvil cell (DAC). Nitrogen was used as the pressure-transmitting medium. Angle-dispersive powder x-ray diffraction patterns (wavelength $\lambda=0.4125$ Å) were measured at the ID09a beamline of the European Synchrotron Radiation Facility, Grenoble, using an image plate detector. The intensity versus 2θ diagrams were obtained by integration using the FIT2D software.[21] To improve powder averaging, the DAC was rotated by ±3°. Raman spectra were recorded in back-scattering geometry, using a micro-Raman spectrometer (LABRAM by Dilor) equipped with a He-Ne laser (632.8 nm), a 20× magnification objective, a holographic notch filter for blocking the laser light, and a CCD detector. For the Raman studies, we initially used a 4:1 methanol/ethanol mixture as the pressure-transmitting me-

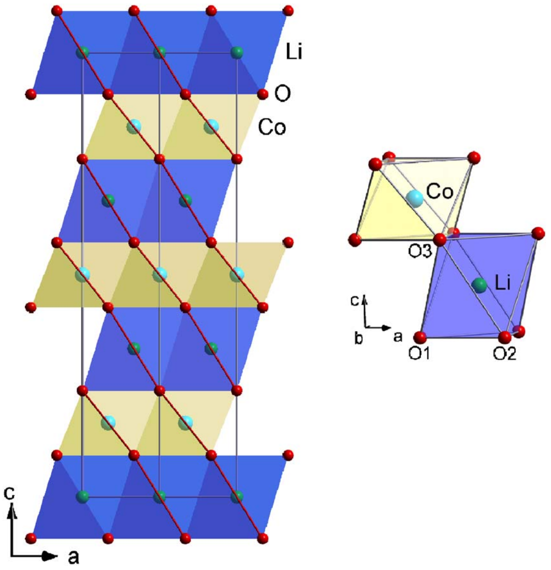

FIG. 1. (Color online) The ambient-pressure crystal structure of the layered form of $LiCoO_2$ (space group $R\bar{3}m$, $Z=1$, Pearson symbol: hR4). The view is along the [110] direction of the hexagonal unit cell. In the hexagonal setting, the oxygen anions occupy the Wyckoff $6c$ $(0,0,z)$ site, and lithium and cobalt cations occupy the $3a$ $(0,0,0)$ and $3b$ $(0,0,0.5)$ octahedral sites. The structure can be derived from rocksalt-type CoO by substituting Li for Co in every second cation layer perpendicular to the cubic [111] direction (which results in a hexagonal supercell cell with $c/a=2\sqrt{6}$) and then allowing for two types of relaxations, a small elongation along the hexagonal [001] axis and a pairing of close-packed oxygen layers described by $z<\frac{1}{4}$. The resulting building blocks are tightly bound O-Co-O slabs separated by layers of lithium atoms. At ambient pressure, the LiO_6 octahedra are about 28% larger in volume than the CoO_6 octahedra.

dium and then checked the reproducibility of data using nitrogen. In all experiments, pressures were measured by the ruby luminescence method.[22]

III. STRUCTURAL PROPERTIES

Selected diffraction diagrams of $LiCoO_2$ at different pressures are presented in Fig. 2(a). A small amount ($\sim 3\%$) of the impurity phase Co_3O_4 was detected; its most intense Bragg peaks are marked by asterisks in Fig. 2(a). The diffraction diagrams also contained a 1% admixture of an unidentified phase, presumably a carbonate; its Bragg peaks are not visible on the scale of Fig. 2(a).

The patterns in Fig. 2 demonstrate that the layered phase of $LiCoO_2$ does not undergo a phase transition within the pressure range up to 26 GPa. The Bragg peaks of $LiCoO_2$ become a little broadened at pressures above 16 GPa. This effect is attributed to nonhydrostaticity caused by the solid nitrogen pressure medium and is not believed to signal a structural instability.

All diffraction diagrams measured for pressures up to 15 GPa were analyzed by full-profile (Rietveld) refinements using the program GSAS.[23,24] The refined parameters were the lattice constants, the atomic position of oxygen, a Chebyshev polynomial background, Pseudo-Voigt profile parameters, and an overall intensity scaling factor. Isotropic thermal parameters for all atom sites were fixed to previously reported ambient-pressure values[8] for all the refinements. A correction for preferred orientation (spherical harmonics model) was applied. Figure 2(b) shows a representative full-profile refinement of $LiCoO_2$ at 9.9 GPa (with impurity-related peaks being masked). Lattice parameters only were extracted from diffraction patterns measured at pressures above 15 GPa. Table I lists refined structural parameters obtained at zero pressure and at 9.9 GPa. Our ambient-pressure results agree with the literature data.[8,9]

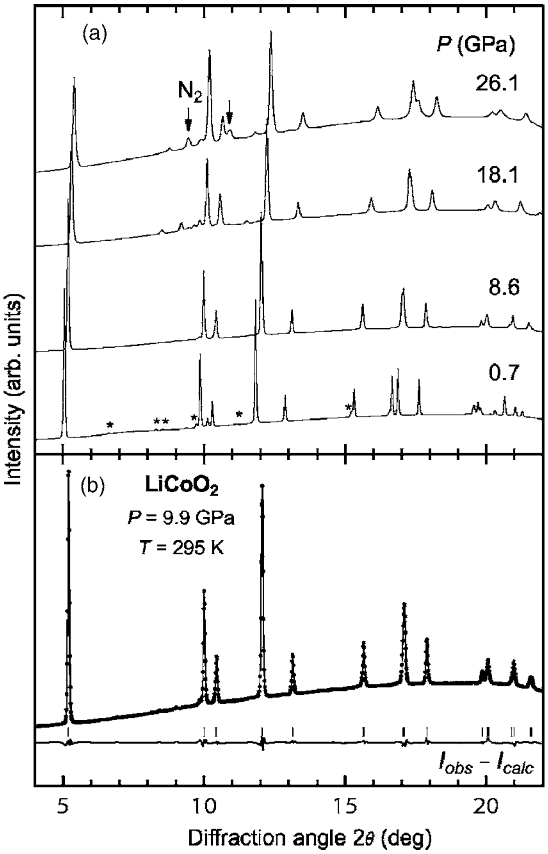

FIG. 2. (a) X-ray powder diffraction patterns of $LiCoO_2$ at selected pressures ($T=300$ K). Arrows mark reflections due to the nitrogen pressure medium. Impurity reflections are marked by asterisks. (b) Rietveld refinement of a pattern measured at 9.9 GPa. Vertical markers indicate the calculated peak positions. The agreement indices of this refinement amount to $R_{wp}=1.6\%$ and $R_p=1.3\%$ (without background).

TABLE I. Structural parameters obtained from full Rietveld refinements of the diffraction diagrams for $LiCoO_2$ collected at ambient pressure and at 9.9 GPa. Data refer to the nonprimitive hexagonal cell with three formula units.

P (GPa)	a (Å)	c (Å)	c/a	z(O)	V (Å^3)
0	2.8155	14.0537	4.992	0.2391(3)	96.48
9.9	2.7732	13.6474	4.921	0.2413(2)	90.89

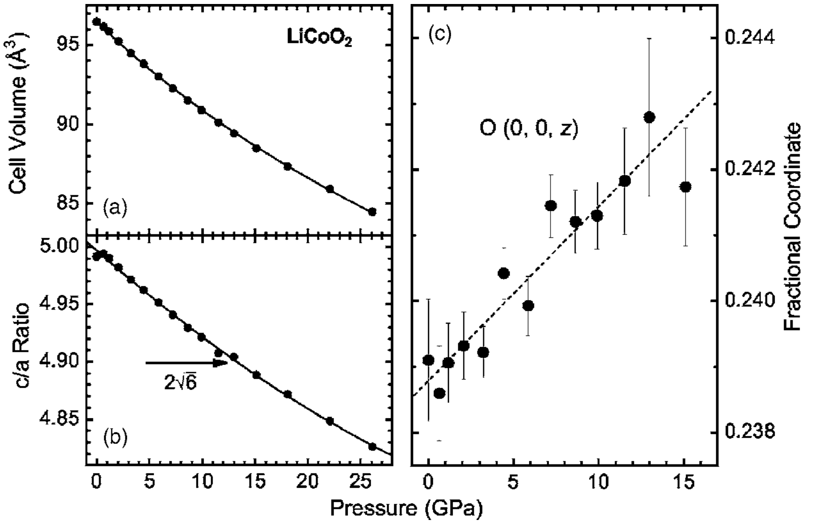

FIG. 3. Structural parameters of $LiCoO_2$ as a function of pressure: (a) Pressure-volume data (symbols) and fitted Birch relation (solid line). (b) Hexagonal axial ratio c/a; the solid line is a guide to the eye, the arrow marks the value of $2\sqrt{6}$ for an ideal close packing of 6 layers. (c) The z parameter of the Wyckoff 6c site of oxygen; the dashed line represents a linear regression.

The full set of refined structural parameters is shown in Fig. 3. By fitting a Birch equation of state[25] to the pressure-volume data [Fig. 3(a)], we obtain values for the zero-pressure bulk modulus B_0 and its pressure derivative B_0' as $B_0=149(2)$ GPa and $B_0'=4.1(3)$. For the fit, the zero-pressure unit cell volume was fixed at the experimental value of $V_0=96.48$ Å^3. The c/a ratio [Fig. 3(b)] is found to drop with increasing pressure. Simultaneously, the oxygen position parameter z increases [Fig. 3(c)]. At about 13 GPa the c/a ratio passes through the "cubic" value of $2\times\sqrt{6}$. At that pressure, the z parameter is still significantly different from $z=\frac{1}{4}$. In other words, the application of pressure does not lead to an ideal cubic-close-packed oxygen sublattice. A linear extrapolation of the $z(P)$ data suggests that the pairing of oxygen layers will be suppressed only at significantly higher pressures than covered in the experiment (see below).

In Fig. 4 the structural parameters are translated into interatomic distances. The fact that the c/a ratio passes through the cubic value at about 13 GPa is equivalent to having all metal-metal distances being equal near that pressure [Fig. 4(a)]. The ambient pressure Li-O and Co-O bond lengths are 2.097(3) Å and 1.918(2) Å, respectively. The Li-O bonds are about three times more compressible than the Co-O bonds [Fig. 4(b)]; the bond length difference extrapolates to zero at the same pressure where the z parameter extrapolates to the value of $\frac{1}{4}$.

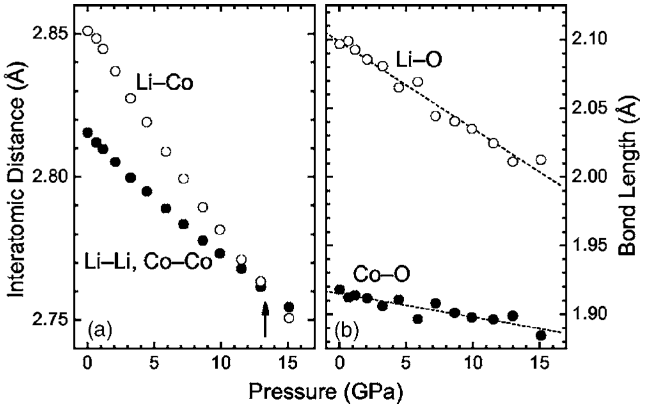

FIG. 4. Interatomic distances in $LiCoO_2$ as a function of pressure. (a) Metal-metal distances Li-Li (Co-Co) and Li-Co. The arrow points to the pressure where all metal-metal distances are equal. (b) Metal-oxygen bond lengths Li-O and Co-O. For comparison, the ambient-pressure Co-O bond length in rocksalt-type CoO (high spin) is 2.132 Å; for antifluorite Li_2O the Li-O bond (tetragonal coordination) is 2.0 Å.

The difference in the Li-O and Co-O bond compressibilities affects the distortions of the octahedral coordinations. As illustrated in Fig. 1, the deviation of the oxygen parameter z(O) from $z=\frac{1}{4}$ describes a compression of the CoO_6 octahedra along c and a corresponding elongation of the LiO_6 octahedra. This type of distortion does not lift the degeneracy of the six intraoctahedral bond lengths. At zero pressure, the LiO_6 octahedra can be characterized by the two distances O(1)-O(2)=2.816(1) Å and O(1)-O(3)=3.098(3) Å and by the two bond angles O(1)-Li-O(2)=84.5(4)°, and O(1)-Li-O(3)=95.4(6)°. With increasing pressures, the difference in O-O distances becomes smaller and the bond angles change towards 90°. For example, at 15 GPa, the bond angles are O(1)-Li-O(2)=86.3(5)° and O(1)-Li-O(3)=93.6(5)°. The CoO_6 octahedra undergo corresponding changes. So, the distortions in both types of octahedra are reduced when applying pressure.

Figure 5 shows the "thicknesses" of the octahedral layers, i.e., their heights projected onto the c axis. Along the c axis direction, the size of the CoO_6 octahedra remains essentially constant; it is the LiO_6 octahedra which are compressed.

IV. RAMAN-ACTIVE PHONON MODES

Turning to the Raman spectroscopy on $LiCoO_2$, Fig. 6 shows selected spectra of $LiCoO_2$ measured at different pressures up to 18 GPa. Two strong modes are observed. Their ambient-pressure frequencies, denoted ω_0 in the following, are 486(1) and 595(1) cm^{-1}, which is in accordance with previous ambient-pressure Raman studies[26,27] of $LiCoO_2$. As expected for nearly stoichiometric $LiCoO_2$, we find no indication for Raman features related to Li vacancies. Impurity-related Raman peaks originating from Co_3O_4 could be

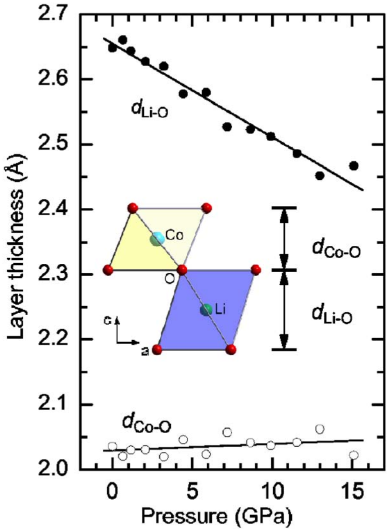

FIG. 5. (Color online) Li-O and Co-O layer thicknesses (projection onto the *c* axis) as a function of pressure.

avoided by selecting a "good" spot on the sample.

The symmetry analysis for $LiCoO_2$ ($R\bar{3}m$, point group D_{3d}) yields the following optical phonon modes at the Γ point: $A_{1g}+2A_{2u}+2E_u+E_g$. The E_g and A_{1g} modes are Raman-active, and the two observed Raman peaks have been attributed to these modes.[26–28] For propagation along the trigonal axis of the rhombohedral lattice, the modes correspond to relative displacements of neighboring oxygen layers with respect to each other, the displacement being along the *c* axis for the A_{1g} mode and perpendicular to *c* for the E_g mode.[27] The two modes can be interpreted as predominantly Co-O stretching and O-Co-O bending motions.[26–28] This interpretation is supported by Li isotope substitution experiments[26] and by comparison to $NaCoO_2$ which occurs in the same layered structure and shows E_g and A_{1g} Raman modes at 486 and 586 cm^{-1}, respectively.[29] Thus, by substituting sodium for lithium, the E_g mode does not shift in frequency (within experimental resolution) and the shift of the A_{1g} mode is quite small, about 9 cm^{-1}.

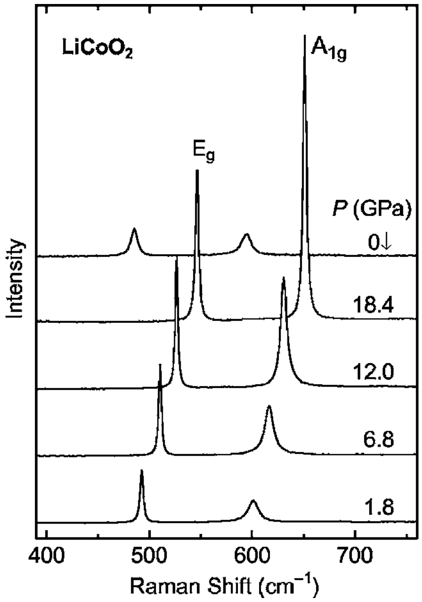

FIG. 6. High-pressure Raman spectra of $LiCoO_2$ measured at room temperature for increasing pressure and after releasing the pressure. The pressure medium was nitrogen.

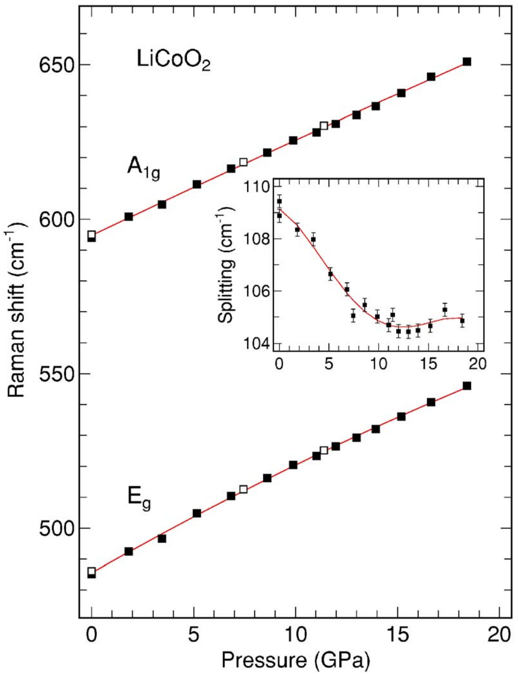

FIG. 7. (Color online) Frequencies of the A_{1g} and E_g Raman modes of $LiCoO_2$ as a function of pressure. Closed symbols are for increasing pressure, open symbols for decreasing pressure. Solid lines refer to fitted results. The inset shows the mode splitting as a function of pressure. There, the solid line is just a guide to the eye.

With increasing pressure, the two Raman modes of $LiCoO_2$ shift to higher frequencies, their absolute intensities increase, the intensity ratio changes, and the linewidths also vary. To quantify these effects, the modes have been fitted by Pseudo-Voigt line shapes.

Within experimental errors, the pressure dependence of the mode frequencies (Fig. 7) can be described by

$$E_g\colon\ \omega(P) = 485.6(7) + 3.75(17)P - 0.0026(9)P^2,$$

$$A_{1g}\colon\ \omega(P) = 594.7(7) + 3.15(18)P - 0.006(9)P^2,$$

where frequency ω is in wavenumbers and pressure P in GPa. Note that the quadratic pressure coefficient for the A_{1g} mode is statistically insignificant. In the range up to 10 GPa the splitting between the A_{1g} and E_g mode frequencies decreases at an average rate of $-0.45\ cm^{-1}/GPa$ (see inset of Fig. 7). Using the definition of the zero-pressure mode-Grüneisen parameter

$$\gamma_0 = -\left(\frac{d\ln\omega}{d\ln V}\right)_{P=0} = \frac{B_0}{\omega_0}\left(\frac{d\omega}{dP}\right)_{P=0}$$

combined with the experimental value of the bulk modulus, the obtained values are $\gamma_0 = 1.15$ for the E_g mode and $\gamma_0 = 0.79$ for the A_{1g} mode.

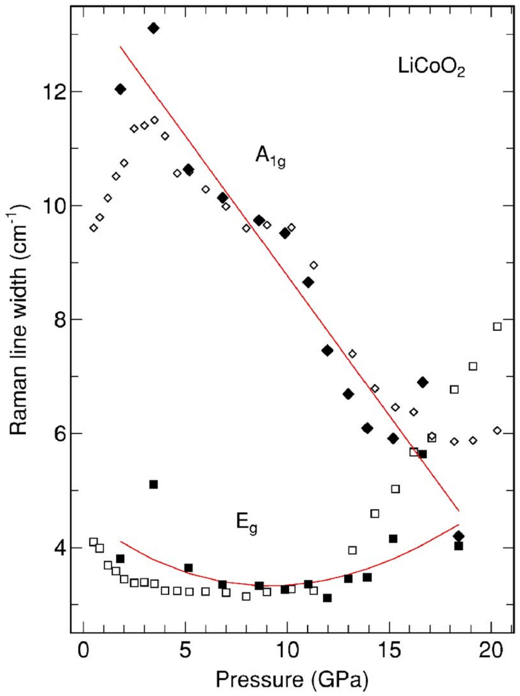

FIG. 8. (Color online) Widths of the A_{1g} and E_g Raman peaks of $LiCoO_2$ as a function of pressure. Open symbols are for the methanol-ethanol pressure medium and closed symbols for the nitrogen medium. Solid lines are guides to the eye. Data were measured using 632.8 nm laser excitation.

The effect of pressure on the Raman linewidths (not corrected for the spectrometer resolution of about 3 cm^{-1} FWHM) is demonstrated in Fig. 8. Data taken in methanol-ethanol and nitrogen pressure medium are shown. Despite some irregular scatter in the data points, presumably caused by inhomogeneity of the sample, overall trends are clearly visible. The width of the E_g peak approaches the resolution limit at pressures from 5 to 10 GPa where the true width of the phonon line must be less than 2 cm^{-1}. At first, it is tempting to attribute the linewidth increase starting at about 12 GPa in 4:1 methanol/ethanol to the solidification of the pressure medium. However, a similar effect is not observed for the A_{1g} mode; on the contrary, its width continues to decrease at pressures beyond 10 GPa. Identifying the physical effects leading to the linewidth changes under pressure, whether caused by anharmonicity or by structural effects not detected in the diffraction measurements, would require a more systematic study using single-crystal samples.

For the given experimental conditions, i.e., 1.96 eV excitation, the integrated intensity of the Raman peaks was observed to increase significantly under pressure (Fig. 6). This effect is more pronounced for the A_{1g} mode (between 0 and 20 GPa its intensity increases by a factor of 7), such that the intensity ratio $R = I_{E_g}/I_{A_{1g}}$ drops from about 0.9 at ambient pressure to ~0.5 at 10 GPa and above. Upon releasing pressure, the intensity changes are largely reversible; this rules out pressure-induced reorientations of the sample as being responsible for the intensity changes. So, it appears that the pressure effects on Raman intensities are induced by changes in the electronic structure.

Optical absorption measurements on thin films of $LiCoO_2$ reveal a prominent absorption band (oscillator strength not specified) at 2.1 eV.[30] In the spirit of earlier theoretical models, the absorption band was attributed to a $t_{2g} \rightarrow e_g^*$ excitation process. The laser energy used in our experiment (1.96 eV) falls slightly below the 2.1 eV band. Depending on the shift of the 2.1 eV feature with pressure, the laser energy may become more or less resonant with electronic transitions. Within the molecular orbital picture of octahedrally coordinated low-spin Co^{3+}, the *average* $t_{2g} - e_g^*$ splitting is expected to increase with decreasing Co-O distance. Within this scenario, which neglects bandwidth and local symmetry changes, an increase in Raman intensity may simply arise from a detuning of a resonance and a related increase in scattering volume. While speculative at this point, the above interpretation is supported by tentative calculations of band gaps of $LiCoO_2$ at two different volumes (see below).

V. CALCULATIONS

We attempted to reproduce the main experimental results on the basis of "total-energy" calculations of $LiCoO_2$ using the density functional theory (DFT). The electronic exchange was treated within, on the one hand, the local density approximation (LDA) and, on the other hand, the generalized gradient approximation (GGA).[31] The calculations employed the VASP implementation of the DFT in a plane-wave basis[32] and used the projector augmented waves (PAW) method.[33,34] Among the PAW potentials for Li, Co, and O provided in the database of Ref. 32 we selected the ones that treat as valence states the outermost 1, 9, and 6 electrons, respectively. Relaxing the $1s^2$ orbital of lithium was not deemed necessary. We are staying within the framework of LDA/GGA and do not consider spin-polarized states as spin polarization was reported previously[35,36] to not have a significant effect on the structural properties of $LiCoO_2$ at ambient conditions.

A plane-wave cutoff of 500 eV has been used and the uniform mesh employed for the Brillouin zone integrations is defined by $(q_1, q_2, q_3) = (4, 4, 4)$ in the notation of Ref. 37. This choice corresponds to ten "special k points" of Monkhorst-Pack.[37] This relatively limited sampling is justified by the semiconducting character of $LiCoO_2$ (Ref. 36) (note that the conduction is ionic, not electronic), a property clearly demonstrated by, e.g., the calculations of the electronic densities of states in Ref. 20. We checked, on all the k points used for Brillouin zone sampling, that even at pressures of the order 30 GPa the gap still does not close.

We obtain, for every atomic configuration, not only the total energy but also the forces acting on all atoms, the stresses acting on the lattice, and the pressure. At every chosen volume we first relax the atomic positions (the oxygen positional parameter z) and then vary the cell shape (the lattice parameters a and c/a) together with z, until the diagonal stresses are equal and forces on all atoms smaller than 10^{-3} eV/Å.

Figure 9 summarizes the main results obtained from the DFT calculations of the structural properties of layered $LiCoO_2$. The calculations were extended to volumes corre-

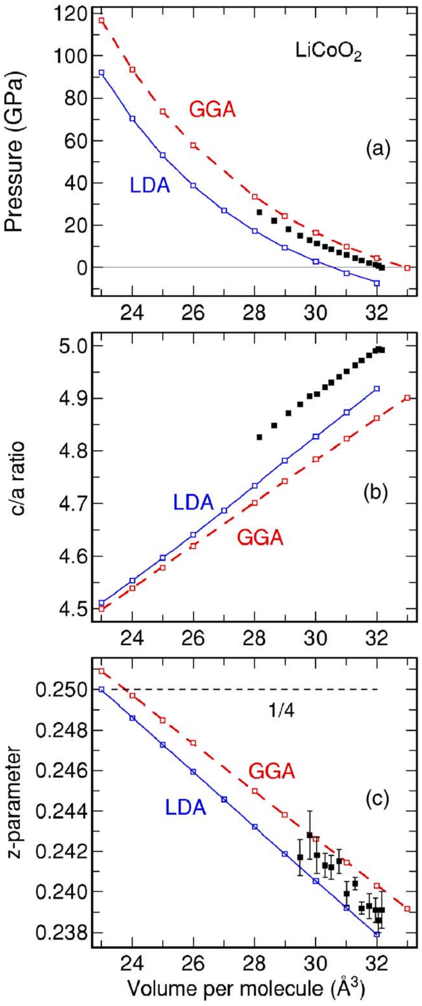

FIG. 9. (Color online) Calculated structural parameters of layered $LiCoO_2$ as a function of volume: (a) Pressure-volume relation; (b) hexagonal axial ratio c/a; (c) the z parameter of the oxygen 6c site. Results for LDA and GGA calculations are given. Experimental data (solid symbols) are included for comparison.

sponding to a pressure of about 100 GPa in order to see how the structural changes would extrapolate if the layered structure is *assumed* to be stable over the whole range. Table II summarizes calculated zero-pressure structural parameters interpolated from the optimizations at different volumes. Again, a fit by a Birch relation was used to determine V_0, B_0, and B_0'.

The LDA and GGA approximations nicely bracket the experimental pressure-volume data, Fig. 9(a). Fitting a Birch equation of state to the calculated PV data in the range between approximately 33 and 23 Å^3/molecule leads to values for the bulk modulus and its pressure derivative as given in Table II.

In both approximations, LDA and GGA, the c/a ratio, Fig. 9(b), comes out somewhat smaller compared to experiment; in fact, the calculated c is a little smaller and the calculated a a little larger than the experimental values. We checked once more in this context that an eventual relaxation of the $1s^2$ electrons in the Li pseudopotential (i.e., treating them as valence states) would *not* fix these discrepancies in c/a.

TABLE II. Structural parameters of $LiCoO_2$ obtained from DFT calculations using the LDA and GGA schemes. Experimental data are listed for comparison. The quoted equilibrium volumes V_0 refer to the primitive rhombohedral cell containing one formula unit. The lattice parameters a and c refer to the nonprimitive hexagonal cell. The quantities B_0 and B_0' were obtained through a fitting of the calculated or experimental $P(V)$ data by a third-order Birch equation of state.

Method	a (Å)	c/a	z(O)	V_0 (Å^3)	B_0 (GPa)	B_0'
LDA	2.7921	4.849	0.2399	30.471	168.5	4.67
GGA	2.8559	4.899	0.2392	32.946	142.9	4.51
Expt.	2.8155	4.992	0.2391	32.16	149(2)	4.1(3)

As for the z parameter, Fig. 9(c), the experimental data are bracketed again. The calculations indicate that the condition $z=\frac{1}{4}$ at which the octahedra around Co and Li become identical can only be achieved at pressures of the order 100 GPa.

Using the frozen-phonon method,[38,39] we have also calculated at different volumes the harmonic frequencies of the two optical phonon modes. Their displacement patterns show that, in both of them, only the oxygen atoms are moving: either "horizontally" (E_g) or "vertically" (A_{1g}), and in the opposite directions. We evaluated the increase in total energy for small displacements $v/a=0.016$ (E_g) and $v/c=\pm 0.004$ (A_{1g}), which amount to ≈ 0.004 and 0.005 Å. The A_{1g} mode turns out to exhibit a weak but non-negligible cubic anharmonicity; in order to eliminate this term we repeated the calculations with + and − displacements ("inward" and "outward" patterns) and averaged the resulting energy changes ΔE. The remaining quartic terms in both power expansions for $E(v)$ can be disregarded because the errors they introduce into the calculated frequencies do not exceed 0.1 to 0.2 cm^{-1}.

Figure 10 shows the frequencies as a function of calculated pressure. In this representation, the absolute frequencies from the LDA and GGA calculations differ by up to 8%. The results provided by the two approximations get considerably closer to each other (to within $\lesssim 1\%$) when plotted as a function of volume. Note, in particular, that the calculated effect of pressure on the mode frequencies compares well with the experimental results.

Anharmonicity of the modes in question is an interesting feature which the frozen-phonon calculations reveal with much more ease than most experiments. As already mentioned, the relation $E(-v)=E(v)$ holds for the E_g mode which means that its lowest anharmonic term is quartic; in the case of the A_{1g} mode the $E(v)$ expansion is marked by the presence of a small cubic term.

Further insight into the anharmonic behavior can be obtained from the knowledge of the forces felt by the displaced atoms; these quantities are provided by the DFT formalism as well. Figure 11 shows the components of the forces acting on one of the displaced oxygen atoms. They are plotted versus the displacement, for both modes and at two different pressures (volumes). The main effect of the displacement, immediately visible in both panels, is the restoring force: that is the largest component, proportional to the displacement and having opposite sign.

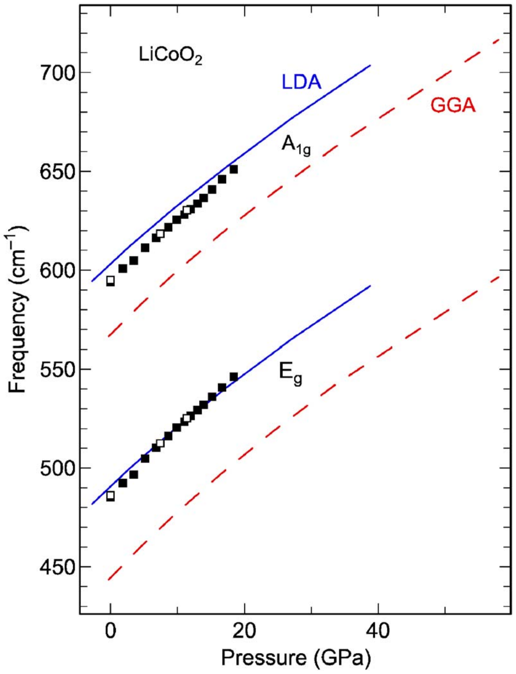

FIG. 10. (Color online) Calculated harmonic phonon frequencies of layered $LiCoO_2$ as a function of calculated pressure. Results for LDA and GGA calculations are given. When plotted as a function of volume, the frequencies provided by the two approximations would differ by $\lesssim 1\%$. Experimental data (symbols) are included for comparison.

A closer inspection of the A_{1g} panel [Fig. 11(a)] reveals that the restoring force is not a perfectly straight line as one would expect from a harmonic oscillator; a small deviation from linearity results from the cubic term $\propto v^3$ in the $E(v)$ expansion; we plotted this contribution separately as "bending" in Fig. 11(a).

In contrast to the A_{1g} case, the restoring force of the E_g mode is exactly linear [Fig. 11(b)], because the cubic anharmonicity is absent from the expansion of $E(v)$ and the *quartic* anharmonicity does not show its presence through a slight nonlinearity. Rather, the restoring force is not exactly parallel to the displacement [which is oriented along $(0,v,0)$], i.e., it also acquires small F_x and F_z components. The slight nonparallelism of displacement and force, a consequence of the anharmonicity of the $E(\boldsymbol{v})$ potential, has already been noticed in earlier DFT calculations of phonons, in a different context.[40]

Also shown in Fig. 11 is the increased slope of the restoring force upon compressing the volume, which correlates with the increase in the eigenfrequency under pressure. Somewhat surprisingly, the anharmonic components (the "bending" of the A_{1g} mode and the F_x, F_z of the E_g mode) hardly vary with pressure.

Altogether, the anharmonic terms are rather small in $LiCoO_2$—at least as far as the above two modes are concerned—in contrast with certain other rhombohedral substances such as, e.g., Sb (see Ref. 41): there, the magnitude of all the above anharmonic phenomena becomes comparable with the restoring force itself and, in addition, the respective anharmonic terms vary considerably with the applied pressure.

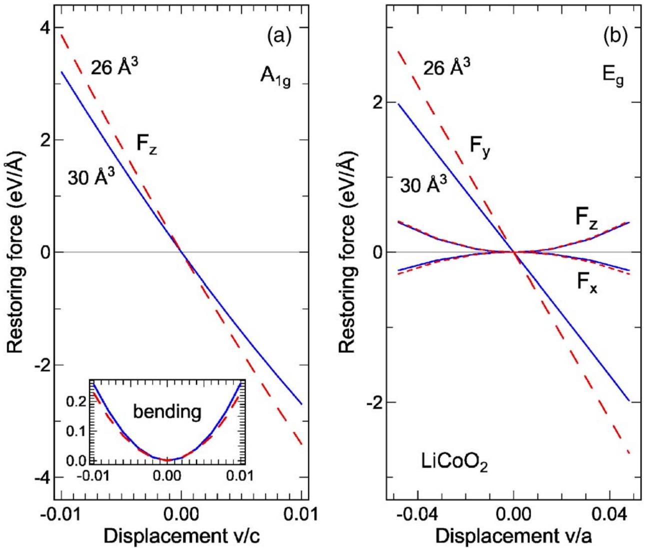

FIG. 11. (Color online) Calculated forces (LDA) as a function of atomic displacements. (a) Restoring forces F_z for the A_{1g} displacement at two different volumes corresponding to pressures of about 0 and 40 GPa. The curves in the inset, marked "bending," indicate the deviations from linear behavior. (b) Forces for E_g-type displacements. In this case the restoring force F_y is linear in the displacement, but there are force components F_x, F_z perpendicular to the displacement direction.

Finally, we briefly comment on the pressure dependence of direct band gaps of $LiCoO_2$. At a unit cell volume of 32 Å^3, the smallest direct gap along any of the high-symmetry lines of the Brillouin zone is calculated to be 1.2 eV within GGA. The fundamental gap located elsewhere in the Brillouin zone is about 0.3 eV lower in energy. At 28 Å^3 the 1.2 eV gap increases by about 0.3 eV. So, the volume deformation potential $dE/d\ln V$ comes out as about −2.4 eV. Similar changes are calculated for other points within the Brillouin zone. The obtained value for the volume deformation potential is relatively small on the scale of deformation potential values for direct gaps in covalently bonded semiconductors.

In the context of our Raman studies it is of interest that the overall trend indeed appears to be an increase of direct gap energies in $LiCoO_2$ with increasing pressure. Therefore, the calculated results are in support of our tentative explanation for the pronounced pressure dependence of the Raman intensities.

VI. SUMMARY

The high-pressure x-ray diffraction studies show that the layered modification ($R\bar{3}m$) of $LiCoO_2$ exists up to at least 26 GPa. Observing no structural phase transformation of layered $LiCoO_2$ occurring at pressures below 26 GPa does not necessarily invalidate the earlier prediction[16] that a cubic spinel-related phase might be thermodynamically more stable at zero temperature and elevated pressures. It could just mean that at room temperature one cannot overcome the high kinetic barriers[35] involved in a redistribution of cations over octahedral sites.

The two structural degrees of freedom of layered $LiCoO_2$, namely the c/a ratio and the oxygen positional parameter z, change in such a way that the LiO_6 and CoO_6 octahedra tend to become more similar under pressure in the geometrical sense.

Total energy calculations performed within density functional theory yield pressure-induced *changes* of structural and elastic parameters in very good agreement with experimental data. Deviations on the absolute scale are within the margins usually encountered when comparing LDA and GGA calculations with experiment (e.g., of the order ±1% in lattice parameters). A brief check of Kohn-Sham eigenvalues calculated at two different volumes indicates that the band gap of $LiCoO_2$ increases under applied pressure.

The pressure dependence of the two Raman-active modes was also investigated. The pressure coefficients of the mode frequencies and the mode-Grüneisen parameters were obtained. While no anomaly is evident in the phonon frequency shifts, a somewhat unusual behavior of peak widths and intensities of both Raman modes is observed. The interpretation of width changes is believed to require a more systematic Raman study using single-crystal samples. The Raman intensity changes may be related to the change in band gap under pressure.

The fact that the layered form of $LiCoO_2$ is found to be *not* susceptible to a pressure-driven structural instability or cation redistribution leads us to suggest that pressure could be an interesting parameter in the study of in-plane vacancy ordering in delithiated Li_xCoO_2 ($x<1$) and other layered cobaltites. Also, staging phenomena[36,42] are expected to be sensitive to pressure, similar to the well-established staging transitions in graphite intercalation compounds.

---

*Electronic address: k.syassen@fkf.mpg.de

[1] K. Mizushima, P. C. Jones, P. J. Wiseman, and J. B. Goodenough, Mater. Res. Bull. **15**, 783 (1980).

[2] J. N. Reimers and J. R. Dahn, J. Electrochem. Soc. **139**, 2091 (1992).

[3] E. Plichta, S. Slane, M. Uchiyama, M. Salomon, D. Chua, W. B. Ebner, and H. W. Lin, J. Electrochem. Soc. **136**, 1865 (1989).

[4] H. F. Gibbard, J. Power Sources **26**, 81 (1989).

[5] T. Nagura and K. Tazawa, Prog. Batteries Sol. Cells **9**, 20 (1990).

[6] R. J. Gummow, M. M. Thackeray, W. I. F. David, and S. Hull, Mater. Res. Bull. **27**, 327 (1992).

[7] R. J. Gummow and M. M. Thackeray, Solid State Ionics **53-56**, 681 (1992).

[8] J. Akimoto, Y. Gotoh, and Y. Oosawa, J. Solid State Chem. **141**, 298 (1998).

[9] H. J. Orman and P. J. Wiseman, Acta Crystallogr., Sect. C: Cryst. Struct. Commun. **40**, 12 (1984).

[10] G. G. Amatucci, J. M. Tarascon, and L. C. Klein, J. Electrochem. Soc. **143**, 1114 (1996).

[11] W. D. Johnston, R. R. Heikes, and D. Sestrich, J. Phys. Chem. Solids **7**, 1 (1958).

[12] A. Marini, V. Berbenni, V. Massarotti, D. Capsoni, and E. Antolini, J. Solid State Chem. **116**, 15 (1995).

[13] S. Levasseur, M. Menetrier, E. Suard, and C. Del, Solid State Ionics **128**, 11 (2000).

[14] N. Douakha, M. Holzapfel, E. Chappel, G. Chouteau, L. Croguennec, A. Ott, and B. Ouladdiaf, J. Solid State Chem. **163**, 406 (2002).

[15] E. Rossen, J. N. Reimers, and J. R. Dahn, Solid State Ionics **62**, 53 (1993).

[16] C. Wolverton and A. Zunger, J. Electrochem. Soc. **145**, 2424 (1998).

[17] Y. Shao-Horn, S. A. Hackney, A. J. Kahaian, and M. M. Thackeray, J. Solid State Chem. **168**, 60 (2002).

[18] J. van Elp, J. L. Wieland, H. Eskes, P. Kuiper, G. A. Sawatzky, F. M. F. de Groot, and T. S. Turner, Phys. Rev. B **44**, 6090 (1991).

[19] M. T. Czyżyk, R. Potze, and G. A. Sawatzky, Phys. Rev. B **46**, 3729 (1992).

[20] M. K. Aydinol, A. F. Kohan, G. Ceder, K. Cho, and J. Joannopoulos, Phys. Rev. B **56**, 1354 (1997).

[21] A. P. Hammersley, S. O. Svensson, M. Hanfland, A. N. Fitch, and D. Häussermann, High Press. Res. **14**, 235 (1996).

[22] H. K. Mao, J. Xu, and P. M. Bell, J. Geophys. Res. **91**, 4673 (1986).

[23] A. C. Larson and R. B. van Dreele, GSAS: General Structure Analysis System, Los Alamos National Laboratory Report LAUR 86-748 (2000).

[24] B. H. Toby, J. Appl. Crystallogr. **34**, 210 (2001), computer program EXPGUI.

[25] F. Birch, J. Geophys. Res. **83**, 1257 (1978).

[26] W. Huang and R. Frech, Solid State Ionics **86-88**, 395 (1996).

[27] M. Inaba, Y. Iriyama, Z. Ogumi, Y. Todzuka, and A. Tasaka, J. Raman Spectrosc. **28**, 613 (1997); C. Julien, Solid State Ionics **157**, 57 (2003).

[28] F. X. Hart and J. B. Bates, J. Appl. Phys. **83**, 7560 (1998).

[29] X. Wang, K. Kunc, I. Loa, and K. Syassen (unpublished).

[30] K. Kushida and K. Kuriyama, Solid State Commun. **118**, 615 (2001).

[31] J. P. Perdew and Y. Wang, Phys. Rev. B **45**, 13244 (1992).

[32] G. Kresse and J. Hafner, Phys. Rev. B **47**, R558 (1993); G. Kresse, Ph.D. Thesis, Technische Universität Wien (1993); G. Kresse and J. Furthmüller, Comput. Mater. Sci. **6**, 15 (1996); G. Kresse and J. Furthmüller, Phys. Rev. B **54**, 11169 (1996).

[33] P. E. Blöchl, Phys. Rev. B **50**, 17953 (1994).

[34] G. Kresse and D. Joubert, Phys. Rev. B **59**, 1758 (1999).

[35] C. Wolverton and A. Zunger, Phys. Rev. B **57**, 2242 (1998).

[36] A. Van der Ven, M. K. Aydinol, G. Ceder, G. Kresse, and J. Hafner, Phys. Rev. B **58**, 2975 (1998).

[37] H. J. Monkhorst and J. D. Pack, Phys. Rev. B **13**, 5188 (1976).

[38] M. T. Yin and M. L. Cohen, Phys. Rev. Lett. **45**, 1004 (1980).

[39] K. Kunc and R. M. Martin, Phys. Rev. B **24**, 2311 (1981).

[40] K. Kunc and P. Gomes Dacosta, Phys. Rev. B **32**, 2010 (1985).

[41] X. Wang, K. Kunc, I. Loa, U. Schwarz, and K. Syassen (unpublished).

[42] Z. Chan, Z. Lu, and J. R. Dahn, J. Electrochem. Soc. **149**, A1604 (2002).